Wetland Mapping and Monitoring with Sentinel-1 and Sentinel-2 Data on the Google Earth Engine

Roshan Kumar Chaudhary[1*], Lila Puri[1], Amul Kumar Acharya[2], Rajaram Aryal[3]

[1]Tribhuvan University, Institute of Forestry Pokhara campus, Pokhara
[1]Tribhuvan University, Institute of Forestry Pokhara campus, Pokhara
[2]Forest Research and Training center, Babar Mahal, Kathmandu
[3]Forest Research and Training center, Babar Mahal, Kathmandu
Correspondence author: Roshan123chy@gmail.com*

ABSTRACT

Wetlands are one of the most valuable ecosystems on the Earth for both humans and nature. Large-scale of wetlands have been transformed into agriculture and urban region in response to human demands and requirements. Accurate mapping and monitoring of large-scale wetlands are of high importance but also challenging. The growing availability of large volumes of open-access satellite data and development of advanced machine-learning algorithms has been providing new opportunities for mapping and monitoring earth system and environment. Google Earth Engine (GEE)- a cloud-based computing platform, has been effectively applied in various areas of mapping ranging from forestry, agriculture, hydrological studies. This study uses high spatial resolution satellite data from Sentinel-1, Sentinel-2 and terrain indices for mapping and monitoring of wetlands of Pokhara Metropolitan city of central Nepal. We implemented different types of wetland classification models on the GEE platform using the Random Forest (RF) classifier. The model with lowest out-of-bag error was chosen as the final model for the preparation of the final classified wetland map. The overall accuracy and kappa coefficient of the classified map were 98% and 0.97 respectively. The study demonstrated the possibility of rapid monitoring of wetlands and other land characteristics using the Google Earth Engine platform.

Keywords: Google Earth Engine, Sentinel-1, Sentinel-2, Random Forest Classifier

INTRODUCTION

Wetlands are one of the most valuable ecosystems on the Earth for both humans and nature. They play a significant role in reducing global greenhouse gas emissions and addressing climate change, while also exerting a substantial influence on biodiversity and the interconnectedness of water systems. (Millennium Ecosystem Assessment, 2005). It is believed that their role contributes essential support to a minimum of seven out of the 17 primary sustainable development goals outlined by the United Nations. (Ramsar Convention Secretariat, 2016). However, the demand and needs of humans have resulted in converting large scale forests, agriculture, and wetland into industrial, settlement and urban land which results in change in precipitation pattern, and drought, dryness of whole ecological system (Millennium Ecosystem Assessment, 2005). Over the past two decades, mapping of wetland has increased due to the better availability of high-quality remote sensing data and tools (Mohammadimanesh *et al., 2016*). However, extensive mapping of wetlands using remote sensing data has always been expensive and challenging (Mohammadimanesh *et al., 2016*).

The increasing accessibility of large volume of satellite data and the advancement in machine learning algorithms have simplified the process of mapping and monitoring the Earth's systems and environment (Mahdianpari *et al., 2019*). This has opened a new avenue for the application of advanced spatial and temporal mapping of wetlands (Hird et al., 2017). The initiation of powerful cloud computing resources such as NASA Earth Exchange, Amazon's Web Service and Google cloud platform have addressed the difficulty of collecting, storing, analyzing, and manipulating multi-temporal ecosystem data of broad geographical region (Mahdianpari, 2019). Google Earth Engine (GEE) is an open-access cloud-based platform which has capability to store and process largescale data (Gorelick *et al., 2017*). It contains an extensive collection of geospatial datasets and satellite images, enabling the development of algorithms and visualizations of results through web-based platforms within a reasonable processing timeframe. (Sazib *et al., 2018*). Besides, to its storage and widely used machine learning algorithms, it allows batch processing using Java Script on a dedicated application programming interface (API) (Kumar & Mutanga, 2018).

Mapping of wetlands of various sizes can play a crucial role in supporting conservation strategies, promoting sustainable management, and facilitating the advancement of wetland mapping at both national and global scales. (Ozesmi & Bauer, 2002). The Copernicus programs of the European Space Agency (ESA) (d'Andrimont *et al., 2018*) produces "12-days SAR Sentinel-2 and 10 days optical Sentinel-2 (multi-spectral Instrument, MSI) images that provides an unprecedented opportunity to collect high spatial resolution data for global wetland mapping" (Mahdianpari, 2019). The primary objective of the Sentinel Missions is to offer comprehensive, unrestricted, and accessible data to the scientific community, enabling worldwide environmental monitoring (Aschbacher & Milagro-Pérez, 2012, (Mahdianpari, 2019). The combined use of Sentinel-1 and Sentinel-2, Earth Observation (EO) data offers new openings to be explored in different applications, especially for mapping phenomena of highly dynamic nature like wetlands (Mahdianpari, 2019).

The development of advanced machine learning tools and geospatial science has contributed for large-scale, reliable, and repeatable wetland mapping and monitoring around the globe (Hird *et al., 2017*). Many studies have demonstrated the potential of fusion of Optical and Synthetic Aperture Radar (SAR) data for the wetland classification (Bourgeau-Chavez *et al., 2015*; Bwangoy *et al.*, 2010; Niculescu *et al., 2020*). The use of SAR data for wetland mapping is critical for monitoring areas with significant cloud cover (Mahdianpari, 2019). This is because SAR sensors are unaffected by overcast and wet conditions and solar radiation. They are more sensitive to the structure, texture, and dielectric properties of land surfaces than optical sensors; (Adeli *et al., 2020*; Sun *et al., 2020*); whereas the optical sensors are sensitive to the reflective and spectral characteristics of ground targets (Mahdianpari, 2019, Mahdianpari, *et al., 2018*). Furthermore, the topography strongly influences the location and size of wetlands, and the reflectance patterns tend to be more reliable and consistent than the surface-vegetation or local-moisture conditions captured by optical and radar backscatter signals (Hird *et al., 2017*). Therefore, for accurate delineation of wetland information, it is possible to bring topographic information and multi-source remote sensing data together for integrated analysis. The goal of the study is to use SAR, topographic, and optical remote sensing data to map and monitor the wetland areas in the Pokhara Metropolitan area.

MATERIALS AND METHODOLOGY

Study Area

This research was carried on the Pokhara Metropolitan City (Fig. 1). It is the administrative center of Gandaki province and is located 200 kilometers west of Kathmandu, Nepal's capital city. It was recently proclaimed the largest metropolitan city, with an area of 464.24 square kilometers. The altitude ranges from 827 meters (2,713 feet) in the southern part to 1,740 meters (5,710 feet) in the northern part. It lies in the Mahabharata Range, Midlands, and the Great Himalayan Range of Nepal between longitudes 83°48'E and 84°13'11"E and latitudes 28°4'39"N and 28°36'18"N. The study area encompasses the basin that has extended from subtropical to the temperate and alpine climates in its northern region. The area receives a high precipitation rate of approximately 3000 mm per year (Rimal *et al, 2013*; Tripathee *et al., 2016)*. This city encompasses nine clusters of lakes (Phewa, Begnas, Rupa, Dipang, Maidi, Khaste, Neurani, Kamalpokhari, and Gunde) of ecological importance listed as 10th Ramsar Site/Wetlands bearing international gratitude and safeguarding the livelihoods and ecosystem.

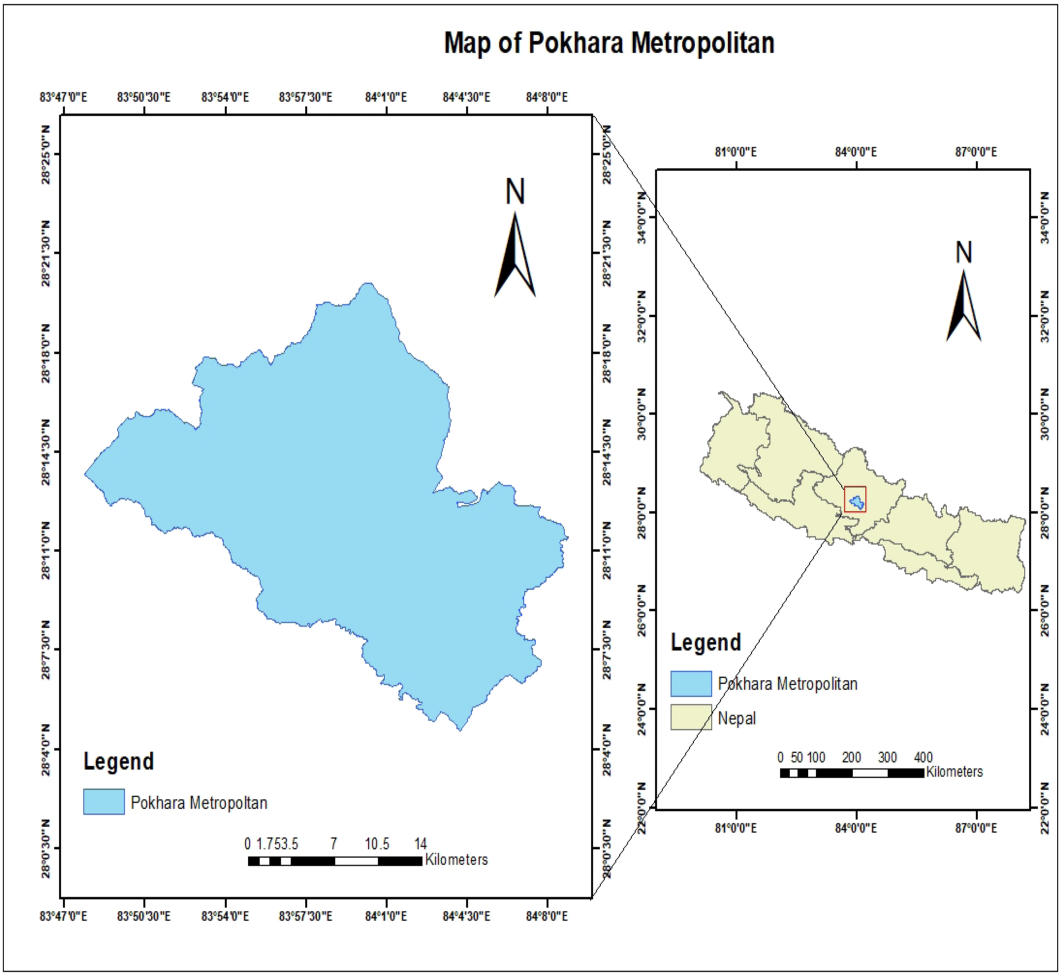

Figure 1: The study Area, Pokhara Metropolitan, Kaski

Data sets and Their Preprocessing

Table 1 summarizes the properties of each of the data set used in this study. The research methodology we followed is proposed by Hird et al. & Sun et al. (Hird *et al., 2017*; Sun *et al., 2020*). We have used spectral band 2 (blue), band 3 (green), band 4 (red), and band 8 (NIR) from the sentinel-2 and used to derive two variables called Normalized Difference Vegetation Index (NDVI) and Normalized Difference Water Index (NDWI) (Mahdianpari, 2019). Three sets of SAR backscatter data from Sentinel-1 SAR C-band Level-1 Ground Range Detected (GRD) images (Sun *et al., 2020*) are vertical-vertical polarization (VV), the standard deviation of vertical-vertical polarization (VVsd) and normalized polarization (POL), and two digital elevation model (DEM)-based topographic indexes as the input for the machine learning model.

Table 1: Overview of Sentinel-1, Senttinel-2 and DEM used for the study.

Data	Derived Variable	Spatial Resolution	Description	Source
Sentinel-1	VV, VVsd, VV-VH/VV+VH (pol) VVrVH	10m	Level-1 Ground Range Detected (GRD), VV and VH polarization (10m)	https://scihub.copernicus.eu/
Sentinel-2	Band2, and3, Band4, Band8, NDVI, NDWI	10m	Visible-Near Infrared optical imagery (10m)	https://scihub.copernicus.eu/
SRTM 1 Arc-Second Global	TWI, TPI	30m	Digital surface model(30m)	https://earthexplorer.usgs.gov/

SAR Imagery

This study uses a total of 138 Sentinel-1 Level-1 SAR pictures in descending orbits. This imagery was collected between May to October of 2018 2019, and 2020 "using the Interferometric Wide (IW) swath mode with a spatial resolution of 10m and a swath of 250km with an average incidence angle of between 30 and 45 degrees" (Mahdianpari, 2019) to calculate the backscatter coefficient for each pixel in the image. GEE already has preprocessed Sentinel-1 radar images in its database, and the following are the processes that GEE takes throughout the preprocessing process (ESA step, 2016; Google Earth Engine, 2020).

1. Applied orbit files.
2. GRD border noise removal.
3. Thermal noise removal
4. Radiometric calibration
5. Terrain Correction

The remaining processing steps were performed using the GEE platform. For Sentinel-1 time-series data, backscatter normalization plays a vital role (Weiß, 2018). The technique that is widely used for this task is the cosine correction method (Hird *et al., 2017*), which was used in this study in terms of the ellipsoidal incidence angles. The normalization of backscatter coefficients was performed because backscatter values of a specific non-wetland area with a small incidence angle returns higher backscatter values than the data of the same are required with a higher incidence angle.

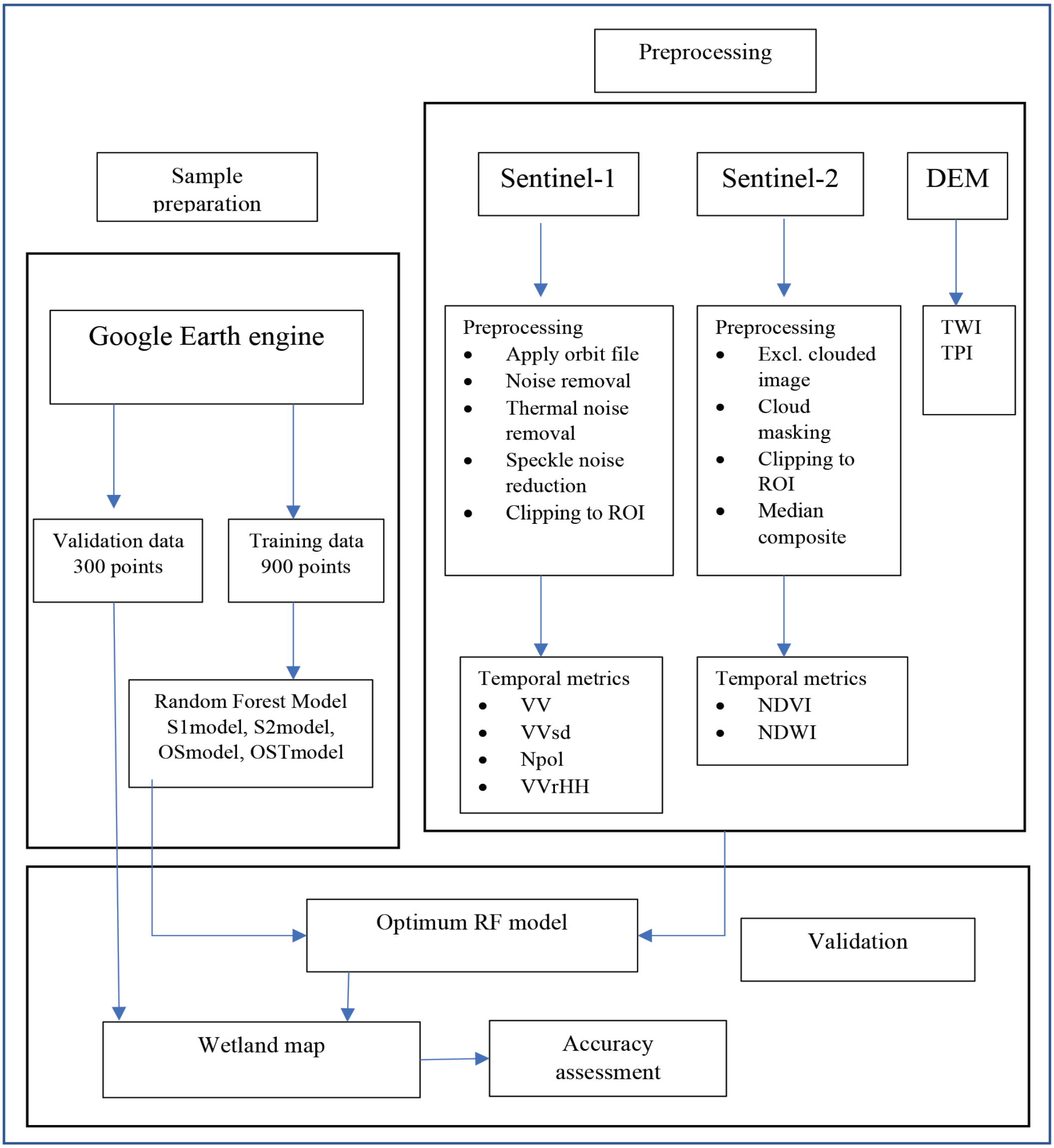

Figure 2: Flowchart of the methodology followed in the study.

Optical Data

The images acquired by Sentinel-2 were a level 2A Bottom of Atmosphere (BOA) product that had been atmospherically adjusted in GEE. Total 13 Sentinel 2A images were used in this mapping process for the mapping of wetland and water bodies. Firstly, low noise and cloud image were filtered by applying selection criteria to cloud percentage less than 20% and the quality assessment band (QA60) was used for cloud masking provided in the metadata of Sentinel product to detect and mask out clouds and circus. To obtain a stable and higher resolution pixel value, the visible bands (red, green, blue and near-infrared) with a resolution of 10m were selected and applied to obtain a multi-year seasonal median image from the collection. The indices that were calculated from the Sentinel-2 images are NDVI and NDWI. NDVI is sensitive to photo synthetically active biomass and can distinguish between vegetation and non-vegetation, as well as between wetland and non-wetland areas (Becker & Choudhury, 1988) while the Normalized Difference Vegetation Index (NDVI. The NDWI was used as additional model input to the NDVI, and it was known to be effective. Its sensitivity to open water has been used in wetland classification as a method of distinguishing land from water (McFeeters, 1996). The normalized difference vegetation index (NDVI) and Normalized Difference Water Index (NDWI) were calculated as follows (McFeeters, 1996):

NDVI = (NIR− Red)/ (NIR+ Red), and

NDWI = (Green − NIR)/ (Green + NIR)

Topographic Data

Topographic position index and Topographic Wetness Index (TWI) were derived using DEM SRTM data obtained from the United States Geological Survey (USGS), which is a worldwide open-access DEM with a spatial resolution of 30 meters (Survey, 2015). To ensure consistency with the remote sensing data, the DEM data was re-gridded to a spatial resolution of 10 meters prior to being used to calculate TWI and Topographic Position Index (TPI). The DEM-based topographic wetness index (TWI) (Wilson & Fothringgham, 2008) and TPI (Beven & Kirkby, 1979) were used to represent the topographic information in this study. TPI indicates the height of each cell (i.e., pixel) in relation to the average elevation of its neighbors. It reflects the topography of the surrounding region and can be used to denote low-lying areas that are wetlands. It is calculated as.

$$TPI=z\_i-\bar{z}r(i)$$

Where *Zi i* is the elevation of pixel or cell and is the average elevation of all the pixels within a given radius, *r*. TWI indicates the potential soil water storage condition of a pixel. It is calculated using an equation taking slope, flow direction, and flow accumulation into account

$$Twi = ln\left(\frac{sCA}{tan\,\phi}\right)$$

Where *SCA* is the special catchment area, and is the slope angle. In this study, we used the open geographic information system (GIS) software System for Automated Geoscientific Analyses (SAGA) (Conrad *et al.*, 2015) to calculate TPI and TWI. The TPI and TWI ranged from-28.2 to 17.6 and from -21.6 to 4.4, respectively.

Multi-year monthly Composite

Several researchers have used Landsat data to create Landsat composite images of a wide region that are almost cloud-free (Flood, 2013; Roy *et al., 2010*) using techniques which will reduce contamination by cloud and other problems. For the purposes of vegetation monitoring, a commonly used technique is the Maximum NDVI Composite, used in conjunction with variety of other constraints. The current paper proposes an alternative based on the medoid (in reflectance space. Few studies have performed thorough examination of Sentinel-2 data for similar studies (Mahdianpari *et al., 2019*). Recent research has also analyzed Landsat data using a variety of composite methods, including seasonal and annual composites (Flood, 2013).

In this research, a Google Earth Engine (GEE) platform was used to create a multi-year seasonal composite of a study area. This was done since the research location is often clouded and rainy, making it difficult to gather enough cloud-free optical data for classification purposes. As a result, we created a multi-year seasonal composite (optical) for spectral signature analysis in order to determine the month with the most semantic information about wetlands and water bodies.

Training and validation sample data

To improve the accuracy and the quality of the final classification of the result, training and validation points are one of the critical steps in the whole process (Millard & Richardson, 2015). Google earth engine has been the main source of information for collecting training and validation data to ensure that training and validation points are represented in the defined land cover classes and avoid the mixed pixel issues.

Three land cover types dominate the area representing land cover class 1 (wetland), 2 (vegetation) and 3 (non-vegetation). For each land cover class, a set of 300 random points were collected for training purposes in the GEE environment. Similarly, a set of 300 validation points (100 in each class) were randomly collected for each study area. All the training and validation points were collected based on high-resolution google earth engine imagery (Gorelick *et al., 2017)*. The sample points were used to perform supervise classification and accuracy assessment. In each model of classification, the following results were generated.

Classification

The classification of different land cover classes can be performed either by pixel or object-based approach. Many studies have been widely demonstrated that object-based approaches can provide more accurate results when using high and very high-resolution data (Cai *et al., 2020*; Mahdianpari *et al., 2019*). In this study, considering the resolution of the image used to carry out the supervised classification, a pixel-based approach was used in this study which has been a widely used approach in the scientific community for the classification of land cover according to Tamiminia *et al. (2020)* narrative. For the mapping of wetland and water bodies, we choose three land cover classes to perform the classification: Wetland and water bodies, vegetation, and non-vegetation land.

Random Forest classification

Random Forest (RF) classifier is considered one of the most widely used algorithms for land cover classification using remote sensing data (Amani *et al., 2019*; Pavlov, 2019; Teluguntla *et al., 2018*). RF is a non-parametric classifier, composed of a group of tree classifiers, and can handle high dimensional remote sensing data (Belgiu & Drăgu, 2016). Random forest is more robust compared to the decision tree algorithm and easier to execute to SVM (Rodriguez-Galiano *et al., 2012*), and another factor making RF more popular than other machine learning algorithms is that only two-parameters (ntree and mtry) are required to be optimized (Maxwell *et al., 2018*). It "uses bootstrap aggregating (bagging) to produce an ensemble of decision trees by using a random sample from the given training data; it also determines the best splitting of the nodes by minimizing the correlation between trees. To assign each pixel it is based on the majority vote of tree can be adjusted by two input parameters namely the number of trees (ntree), which is generated by randomly selecting samples from the training data, and the number of variables (m try), which is used for tree node splitting" (Pavlov, 2019, Mahdianpari, 2019).

In this study, the Random Forest (RF) algorithm was used to train and predict the wetland and water bodies of Pokhara Municipality. Large-analysis of 349 GEE peer-review articles over the last 10 years shows that the RF algorithm is the most frequently used classification algorithm for satellite imagery (Tamiminia *et al., 2020*). Taking into consideration all the reasons, we chose RF for the present study. Based on a trial-and-error approach, the parameter n-tree was assessed for the following values for each model (a) 100, (b) 200, (c) 400, (d) 500 while n-tree was set to the default value (square root of the total number of features). A value of 300 was then found to be appropriate in this study, with the lowest OOB (out of bag error) as shown in table 3.

RESULTS

Classified Wetland map with different input variable

The entire study design consists of three stages, as shown in Figure 2. The workflow's initial step is to preprocess all acquired data. The Sentinel-1 and Sentinel-2 images were processed in Google Earth Engine, while the TPI and TWI were obtained from the DEM using the SAGA software. The accuracies of RF models are illustrated in table 2. The percentage of wetland pixels based on the S2 model as shown in Figure 3(b) was 3.18 percent, followed by vegetation pixels, which was 57.2 percent and non-vegetation pixels, which was 39.5 percent. The percentage of wetland pixels in the OSmodel, which is presented in the Figure 3(c), is 2.98 percent, with the pixel covering 57.23 percent of the vegetation area and 39.78 percent of the non-vegetation pixels. Similarly, the OST model as shown in the Figure 3(d) revealed the lowest percentage of wetland pixels (2.94%) while it was highest for vegetation (57.78%) followed by non-vegetation pixel (39.28%) of the study region. Furthermore, the S1model Fig. 4(a) detected more pixels of wetland than the combined results of the two previous models. Wetland area accounted 8 percent of the total area while it was 54.8 percent for vegetation and 37 percent for non-vegetation. The overall accuracies of the S1model and S2model, was lower (77%) compared to other models which was 98 percent as shown in the table 2. Consequently, the OSTmodel was chosen to predict the final wetland map of the Pokhara Metropolitan city based on the OOB error.

Table 2 : Overall Accuracies, out-of-bag (OOB) error and Kappa coefficient of different classification model.

RF Model	ntrees	OOB	Overall Accuracy	Kappa coefficient
S1model	300	0.1988	77%	0.66
S2model	300	0.015	98%	0.97
OSmodel	300	0.02	98%	0.97
OSTmodel	300	0.015	98%	0.97

Classification accuracies of different models

We calculated the producer-user relationship and the overall accuracy of several models based on the Random Forest classifier. We used the identical training sample and validation data points for all models and evaluated the classification accuracy of wetlands and water bodies. The accuracy of several models is summarized in Table 3.

S1 model

The overall accuracy of the S1 model was 77 percent, while the producer accuracy and user accuracy of the S1 model for wetland class were 93 percent and 83 percent, respectively. Additionally, the vegetation class has consumer accuracy of 77% and producer accuracy of 73%, respectively. In the same way, the consumer accuracy of the non-vegetation class was 71 percent, and the producer accuracy was 67 percent.

S2 model

The overall accuracy of the S2model was 98 percent, with consumer accuracy in the class wetland being 99 percent and producer accuracy being 99 percent. In a similar manner, the vegetation class contains producers with 100 percent accuracy and consumers with 96 percent accuracy, whereas the non-vegetation class contains producers with 98 percent accuracy and consumers with 95 percent accuracy.

OS model

The overall accuracy of the OSmodel was 98 percent, with the wetland class achieving producer accuracy of 99 percent and consumer accuracy of 99 percent in the process. A 100 percent classification accuracy for producers and a 95 percent classification accuracy for consumers were obtained in the vegetation class. Similarly, the consumer accuracy for the non-vegetation class was 99 percent, while the producer accuracy was 100 percent.

OST model

OST model achieved an overall accuracy of 98 percent, with the wetland class including producers with accuracy of 100 percent and consumers with accuracy of 99 percent. Vegetation class with producer accuracy of 100 percent and consumer accuracy of 96 percent. Similar to the non-vegetation class, producer accuracy was 95 percent, and consumer accuracy was 100 percent in the non-vegetation class.

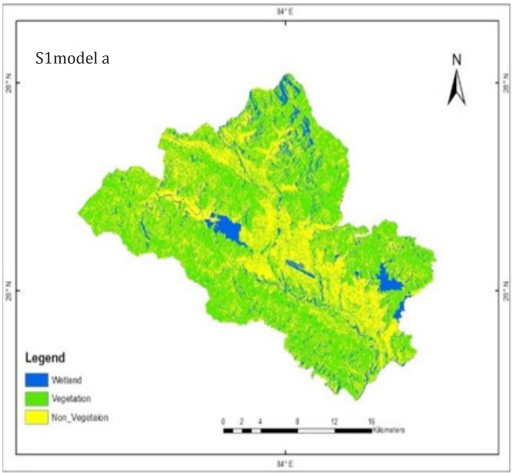

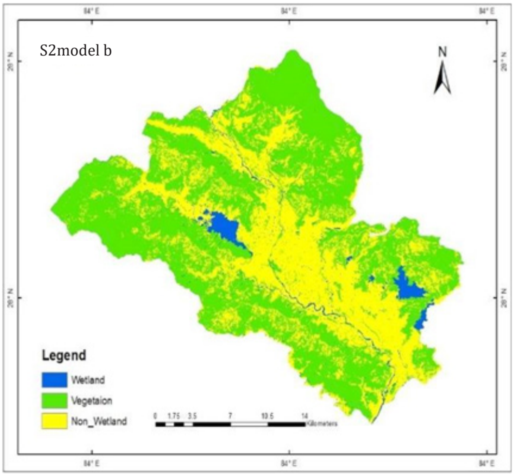

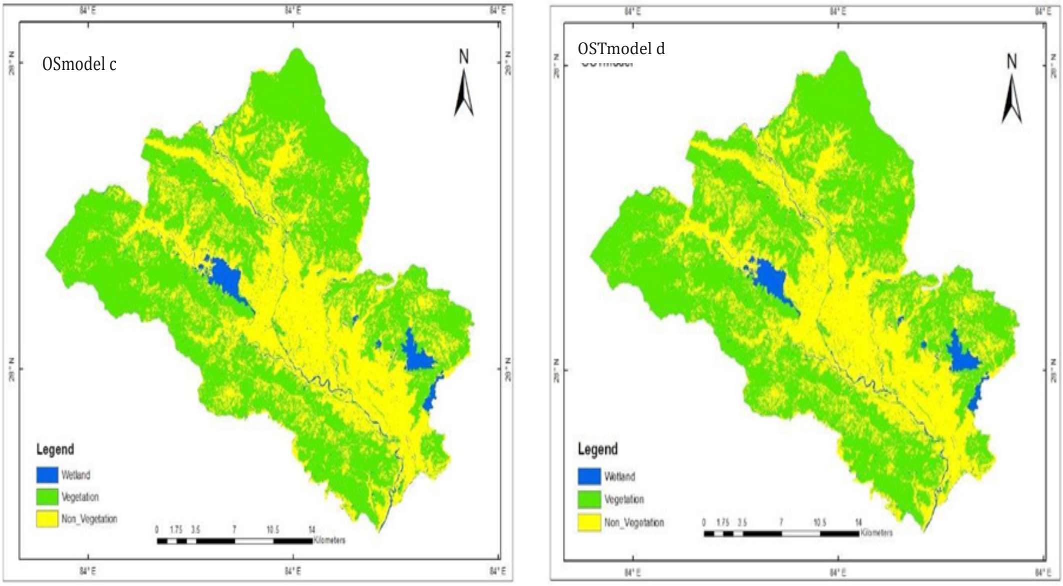

Figure 3: The Classified Map of Different Models

Models	Wetland		Vegetation		Non-vegetation		OA (%)
	UA	PA	UA	PA	UA	PA	
S1	83	93	77	73	71	67	77
S2	99	99	96	100	98	95	98
OS	99	99	95	100	98	95	98
OST	99	100	96	100	100	95	98

Table 3: Showing the User accuracies and Producer accuracies of different model.

Variable Importance of Different model

Figure 5 shows a summary of the impact of different parameters on the achievement of classification using Random Forest classification. Observations have shown that the variables that are important have a high rank of significance. The NDWI and the NDVI are the most significant indices in the identification of wetland and water bodies as well as vegetation and non-vegetation classes. Similarly, the indices VVmean, VVsd, Npol, VVrVH are the most essential for distinguishing wetland and water bodies, respectively.

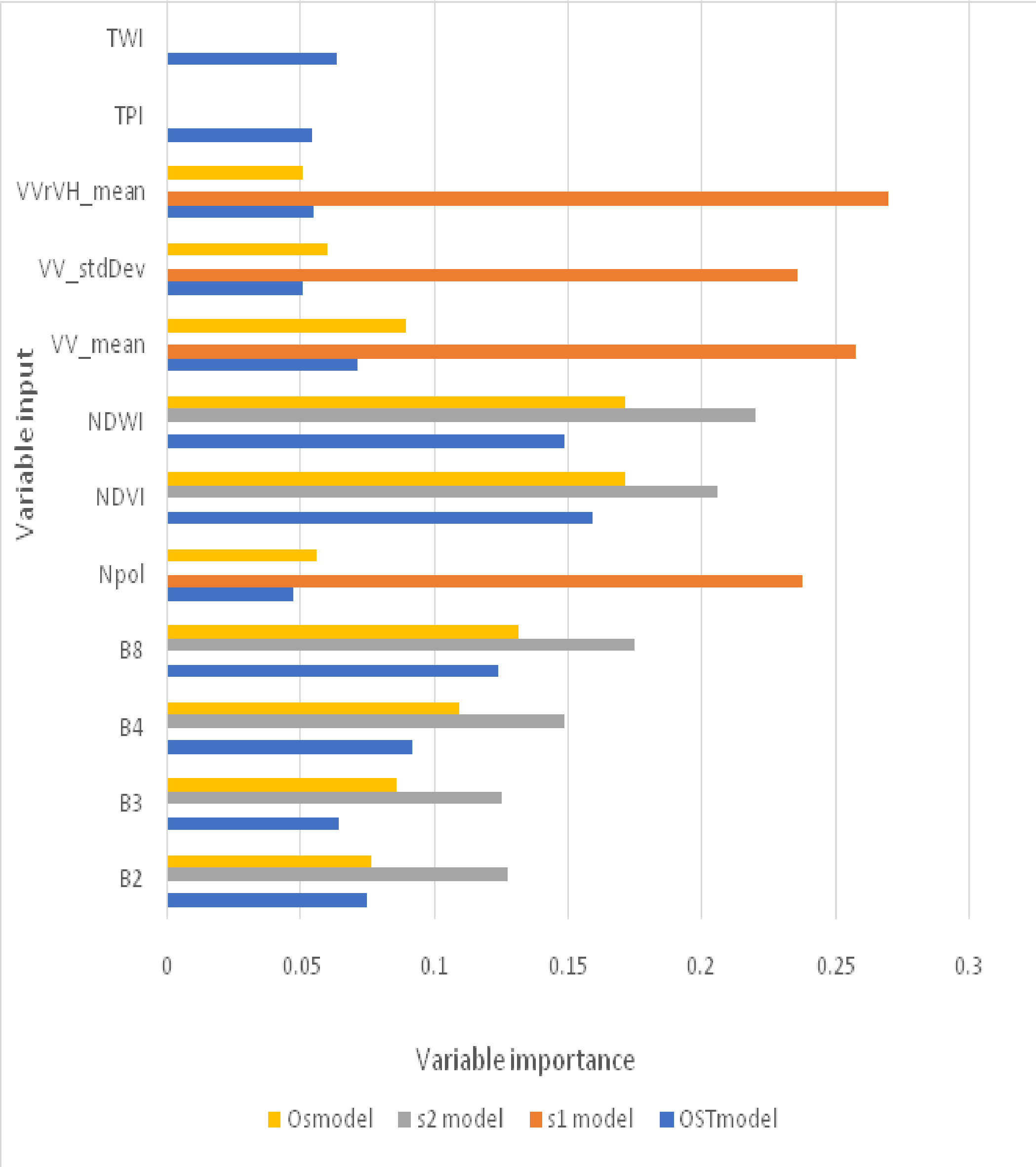

Figure 4: Variable importance of different input variable used in different models.

Spectral analysis of multi-year monthly composite

To evaluate the capability of various spectral bands and vegetation indicators, spectral analysis of all land cover classes was conducted. Figure 5 shows the statistical distribution of reflectance for NDVI, NDWI, and other visible band of monthly composites from October, November, and December 2018 to 2020.

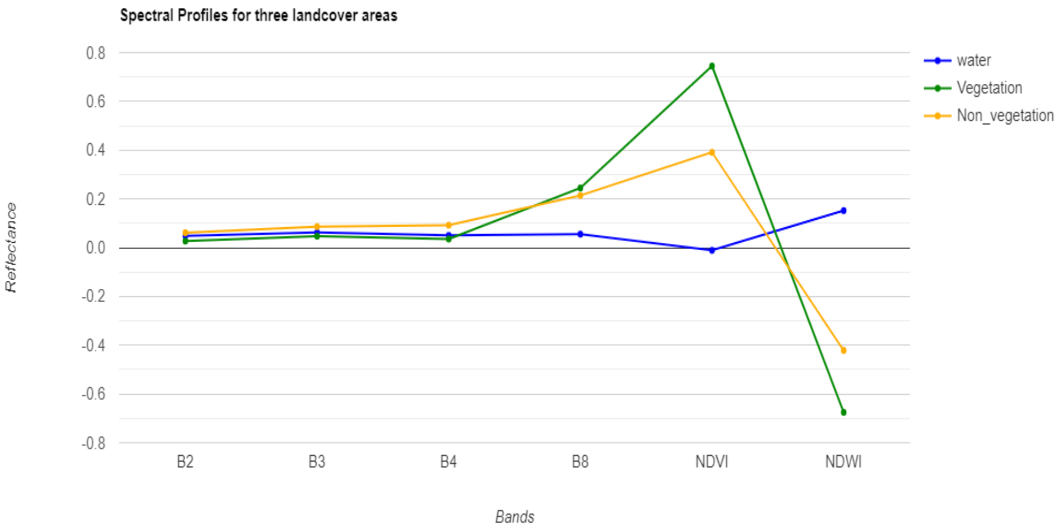

Figure 5: Spectral analysis of multi-year monthly composite curve

As demonstrated, all visible bands are unsatisfactory in distinguishing between wetland and water bodies, whereas vegetation indices, such as the NDVI, are superior in distinguishing between vegetation and non-vegetation. Similarly, NDWI is critical in distinguishing wetlands and water bodies from other land covers. Furthermore, the use of NIR bands has been shown to be useful in distinguishing between various land cover classifications.

Variation of area per classes in different model

The area corresponding to each land cover class was determined using the results of various models we looked at. According to the S2 model, the wetland area was 14.84 hector, the vegetation area was 266.43 hector, and the non-vegetation area was 184.40 hector. Similarly, the S1 model resulted in more wetland area than the combined results of the other models, with wetland area accounting for 37.43 hectors, vegetation area by 255.66 hectare and non-vegetation other area by 172.58-hectare. While wetland coverage in the OSmodel resulted 13.89 hector, it was 266.53 hectors for vegetation and 185.25 hectares for non-vegetation areas. The OST model also revealed the smallest wetland area, which was 13.67 hectors, while it was highest for the vegetation area, which is 269.05 hectares and non-vegetated area which was, 182.91 hectares. Comparing the classification results with the ESRI land cover 2020 map, it can be seen that vegetation land has the highest land cover area with 303.29 hectares, followed by non-vegetation at 147.82 hectares and wetland at 14.54 hectares.

Table 4: Area of different land cover class in hectares

Land cover	Area of different land cover in hectares				
	S1model	S2model	OSmodel	OSTmodel	ESRI land cover
Wetland	37.43	14.84	13.89	13.67	14.54
Vegetation	255.66	266.43	266.53	269.05	303.29
Non-Vegetation	172.58	184.40	185.25	182.91	147.82

Evaluation of Classified map

Table 3 displays the overall accuracies (OA) and kappa coefficient for various classification scenarios. The utilization of optical imagery yielded more favorable classification outcomes compared to SAR imagery (Mahdianpari, 2019). As illustrated, the optical imagery (S2model) resulted higher accuracy compared to the radar imagery (S1model).

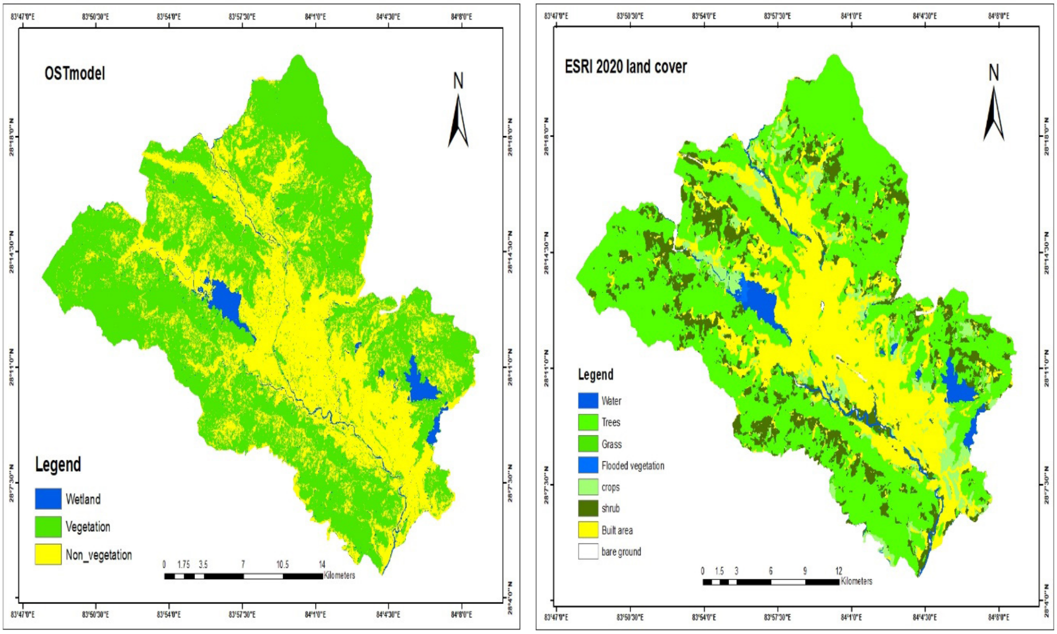

(a) (b)

Figure 5 . Classified map (a) OST Model and Esri land cover map 2020 (b).

The final classified map was created using the OSTmodel, which incorporates optical, radar and topographic data. We obtained an overall accuracy of 98 percent and a Kappa coefficient of 0.97. This model was chosen based on the random classifiers out-of-bag (OOB) error. For the classification of wetlands and water bodies, the model with the lowest out-of-bag error was chosen.

Figure 5(a) is the final classified map using OST model for the study area. We compared the wetland and water bodies of Pokhara Metropolitan map with the ESRI Global land cover map of 2020, Fig. 5(b). The findings indicated that patterns of the two wetlands maps were comparable in identifying water bodies. Nevertheless, there were minor variation in them. Therefore, our data indicated that total area of wetlands of Pokhara were larger than the ESRI land cover map of 2020. The total area of water bodies was 14.54 ha in the ESRI global land cover map 2020 (Karra *et al.*, 2021).

DISCUSSION

The variable importance and spectral analysis results showed that the NIR band is superior to the visible band (blue, green, and red) for identifying wetland. When it comes to vegetation indexes, the NDVI has shown to be the most helpful. This result is explained by the fact that the NDVI is very sensitive to photosynthetically active biomass in the environment (Xiong *et al., 2017*). The obtained variable importance values indicate that the optical variable NDWI was considerably higher than the radar variables. When it comes to recognizing water bodies and other land cover classifications, the Synthetic Radar Aperture (SAR) indices VVmean and the ratio of VV and VH (VVrVH) are significant. As our results demonstrate, the pixel percentage of wetland class in Sentinel-1 is significantly higher than that in the S2model. The result concures with other studies which have demonstrated that Sentinel-1 has great potential for monitoring dynamics changes in water surface area and providing more detailed information about temporal classification, such as classification of flood frequencies or surface water dynamic (Tian *et al.*, 2017; Xing *et al.*, 2018).

In the classification for general wetland delineation, the accuracy of sentinel-2 and the combined use of Sentinel-1 and Sentinel-2 were satisfactory, while the accuracy of the sole use of Sentinel-1 was quite low, as shown in table 3. The advantage of optical images over SAR images is seen across all evaluation indices in this research. It suggests that optical indices (e.g., NDVI) and the difference between water and non-water classes represented by the NDWI index are more effective for wetland mapping than the feature derived from dual-polarimetric SAR data. The finding is consistent with the result of earlier research (Hird *et al., 2017*; Mahdianpari 2019). The finding from (Mahdianpari *et al., 2019*)highlighted that there is limited capacity of Sentinel-1 C-band sensors operating in VV/VH mode capture difference in forest and high-vegetated wetlands. Earlier studies have revealed use of the L- or P-band radar system and

HH polarization are more suitable for this purpose (Wang *et al., 1995*). Advanced SAR-based information products, such as decomposition techniques for removing scatter processes, would be useful in gaining a more deep understanding of the function that SAR data may play in a modelling approach(Furtado *et al., 2016*; Mahdianpari *et al., 2017*).

Although optical data were superior to SAR, higher classification accuracy was achieved while SAR composites were integrated with the optical and topographical composites. This is because the optical and SAR data are based on the range and angle measurement and gather data on the chemical and physical properties of the wetland vegetation (Chen *et al., 2017*). As a result, including both kinds of observations improves the discriminating of backscattering or spectrally similar wetland classes (Van Beijma *et al., 2014*). The combination of SAR, optical composite, and topographic data were shown to be extremely beneficial for increasing overall classification accuracy in previous studies (Hird *et al., 2017*), despite the fact that the OSmodel and OSTmodel produced very similar results in our study.

When employing the image mosaicking method over a lengthy time period is required, it is possible that classification mistakes may rise in regions with substantial inter-annual variation (Kelley *et al., 2018*). Although this image mosaicking method is critical for overcoming the constraint of frequent cloud cover when mapping land cover using optical remote sensing data at a large geographical scale, this constraint was reduced to a reasonable extent in our research. The use of such multi-year seasonal composites has previously been emphasized, given their ability to capture surface condition changes useful for wetland mapping.

CONCLUSION

As a consequence of recent advancements in geospatial science, "cloud-based computing resources and open-access EO data have spurred a paradigm shift in the field of land cover mapping" (Mahdianpari, 2019), replacing static maps with more dynamic and application-specific maps. Using Google Earth and Copernicus Sentinels high spatial resolution remote sensing data, this study produced the first map of wetlands and water bodies in the Pokhara Metropolitan region of Nepal, using multi-year monthly composite sentinel-1, sentinel-2, and topography data.

In this research, we created a process for mapping and monitoring the wetland in the study region, which was based on the Google Earth Engine cloud-based platform and made use of the random forest classifier, open-access and multiple remote sensing data, as well as topographic information form digital elevation model. The classified map that was generated with overall accuracy of 98 %, kappa coefficient of 0.97 and out-of-bag error of 0.015. The research showed the feasibility of monitoring wetland and other land features quickly utilizing the GEE platform, machine learning techniques, and currently available high-resolution satellite data.

ACKNOWLEDGEMENT

I would like to acknowledge my advisor and co-advisor for their continuous guidance and advice throughout this research. I also would like to thank Shaobo Sun of Institute of Surface-Earth System Science, School of Earth System Science, Tianjin University who has helped me coding in google earth engine.

REFERENCES

Adeli, S., Salehi, B., Mahdianpari, M., Quackenbush, L. J., Brisco, B., Tamiminia, H., & Shaw, S. (2020). *Wetland Monitoring Using SAR Data: A Meta-Analysis and Comprehensive Review.* Remote Sensing, 12(14), 2190. https://doi.org/10.3390/rs12142190

Amani, M., Mahdavi, S., Afshar, M., Brisco, B., Huang, W., Mirzadeh, S. M. J., White, L., Banks, S., Montgomery, J., & Hopkinson, C. (2019). *Canadian Wetland Inventory using Google Earth Engine: The First Map and Preliminary Results.* Remote Sensing, 11(7), 842. https://doi.org/10.3390/rs11070842

Assessment, M. E. (2005). *Ecosystems and human well-being: wetlands and water.* World Resources Institute, Washington, DC.

Baghdadi, N., Bernier, M., Gauthier, R., & Neeson, I. (2001). *Evaluation of C-band SAR data for wetlands mapping.* International Journal of Remote Sensing, 22(1), 71–88. https://doi.org/10.1080/014311601750038857

Becker, F., & Choudhury, B. J. (1988). *Relative sensitivity of normalized difference vegetation Index (NDVI) and microwave polarization difference Index (MPDI) for vegetation and desertification monitoring.* Remote Sensing of Environment, 24(2), 297–311. https://doi.org/10.1016/0034-4257(88)90031-4

Belgiu, M., & Drăgu, L. (2016). *Random forest in remote sensing: A review of applications and future directions.* ISPRS Journal of Photogrammetry and Remote Sensing, 114, 24–31. https://doi.org/10.1016/j.isprsjprs.2016.01.011

Beven, K. J., & Kirkby, M. J. (1979). *A physically based, variable contributing area model of basin hydrology.* Hydrological Sciences Bulletin, 24(1), 43–69. https://doi.org/10.1080/02626667909491834

Cai, Y., Pan, Q., Zhang, M., & Lin, H. (2020). *Mapping wetland using the object-based stacked generalization method based on multi-temporal optical and SAR data.* International Journal of Applied Earth Observation and Geoinformation, 92, 102164. https://doi.org/10.1016/j.jag.2020.102164

Chen, B., Xiao, X., Li, X., Pan, L., Doughty, R., Ma, J., Dong, J., Qin, Y., Zhao, B., Wu, Z., Sun, R., Lan, G., Xie, G., Clinton, N., & Giri, C. (2017). *A mangrove forest map of China in 2015: Analysis of time series Landsat 7/8 and Sentinel-1A imagery in Google Earth Engine cloud computing platform. ISPRS Journal of Photogrammetry and Remote Sensing,* 131, 104–120. https://doi.org/10.1016/j.isprsjprs.2017.07.011

Conrad, O, B. Bechtel, B, Bock, M, H. Dietrich, H, Fischer, E, L. Gerlitz, Wehberg, J, Wichmann, V, & J. Bohner, J (2015). *System for Automated Geoscientific Analyses (SAGA)* v. 2.1.4, Geoscientific Model Development, 8, 1991-2015

d'Andrimont, R., Lemoine, G., & van der Velde, M. (2018). *Targeted grassland monitoring at parcel level using sentinels, street-level images and field observations.* Remote Sensing, 10(8), 1–27. https://doi.org/10.3390/RS10081300

Platform, S. A. (2017). European Space Agency (ESA). *Science Toolbox Exploitation Platform.* Available online: http://step. esa. int/main/toolboxes/snap/(accessed on 23 June 2015).

Flood, N. (2013). *Seasonal composite landsat TM/ETM+ Images using the medoid (a multi-dimensional median).* Remote Sensing, 5(12), 6481–6500. https://doi.org/10.3390/rs5126481

Furtado, L. F. de A., Silva, T. S. F., & Novo, E. M. L. de M. (2016). *Dual-season and full-polarimetric C band SAR assessment for vegetation mapping in the Amazon várzea wetlands.* Remote Sensing of Environment, 174, 212–222. https://doi.org/10.1016/j.rse.2015.12.013

Gherboudj, I., Magagi, R., Berg, A. A., & Toth, B. (2011). *Soil moisture retrieval over agricultural fields from multi-polarized and multi-angular RADARSAT-2 SAR data.* Remote Sensing of Environment, 115(1), 33–43. https://doi.org/10.1016/j.rse.2010.07.011

Google Earth Engine. (2020). *A planetary-scale platform for Earth science data & analysis. Available at: Https://Earthengine.Google.* Com/(Accessed: 04/05/2020). https://earthengine.google.com/

Gorelick, N., Hancher, M., Dixon, M., Ilyushchenko, S., Thau, D., & Moore, R. (2017). *Google Earth Engine: Planetary-scale geospatial analysis for everyone.* Remote Sensing of Environment, 202 (2016), 18–27. https://doi.org/10.1016/j.rse.2017.06.031

Hird, J. N., DeLancey, E. R., McDermid, G. J., & Kariyeva, J. (2017). *Google Earth Engine, Open-Access Satellite Data, and Machine Learning in Support of Large-Area Probabilistic Wetland Mapping.* Remote Sensing, 9(12), 1315. https://doi.org/10.3390/rs9121315

Integrity, S., Cluster, L., & Valley, P. (2016). *Integrated Lake Basin Management Plan of Lake Cluster of Pokhara Valley, Kaski, Nepal.* Integrated Lake Basin Management Plan of Lake Cluster of Pokhara Valley, Nepal (2018-2023), December.

Karra, K; Kontgis, C; Statman-Weil, Z; Mazzariello, J; Mathis, M; Brumby, S. (2021). *Global land use/land cover with Sentinel-2 and deep learning, IGARSS 2021-2021 IEEE International Geoscience and Remote Sensing Symposium.* IEEE, 2021, Impact Observatory, United States

Kelley, LC, Pitcher, L & Bacon, C (2018). *Using Google Earth Engine to Map Complex Shade-Grown Coffee Landscapes in Northern Nicaragua, Remote Sensing,* 10(6), 952; https://doi.org/10.3390/rs10060952

Kumar, L., & Mutanga, O. (2017). *Remote Sensing of Above-Ground Biomass.* Remote Sensing, 9(9), 935. https://doi.org/10.3390/rs9090935

Kumar, L., & Mutanga, O. (2018). *Google Earth Engine applications since inception: Usage, trends, and potential.* Remote Sensing, 10(10), 1–15. https://doi.org/10.3390/rs10101509

Mahdavi, S., Maghsoudi, Y., & Dehnavi, S. (2014). *A method for soil moisture retrieval in vegetated areas using multi-frequency data considering different kinds of interaction in different frequencies.* Proceedings of the European Conference on Synthetic Aperture Radar, EUSAR, Proceeding(November), 755–758. https://doi.org/10.13140/2.1.3459.7441

Mahdavi, S., Salehi, B., Granger, J., Amani, M., Brisco, B., & Huang, W. (2018). *Remote sensing for wetland classification: a comprehensive review.* GIScience and Remote Sensing, 55(5), 623–658. https://doi.org/10.1080/15481603.2017.1419602

Mahdianpari, M., Granger, J., Mohammadimanesh, F., Salehi, B., Brisco, B., Homayouni, S., ... Lang, M. W. (2020). *Meta-Analysis of Wetland Classification Using Remote Sensing: A Systematic Review of a 40-Year Trend in North America.* Remote Sensing, 12(11), 1882. https://doi.org/10.3390/rs12111882

Mahdianpari, M., Salehi, B., Mohammadimanesh, F., Homayouni, S., & Gill, E. W. (2018). *The First Wetland Inventory Map of Newfoundland at a Spatial Resolution of 10 m Using Sentinel-1 and Sentinel-2 Data on the Google Earth Engine Cloud Computing Platform.* Remote Sensing, 11(1), 43. https://doi.org/10.3390/rs11010043

Mahdianpari, M., Salehi, B., Mohammadimanesh, F., & Motagh, M. (2017). *Random forest wetland classification using ALOS-2 L-band, RADARSAT-2 C-band, and TerraSAR-X imagery.* ISPRS Journal of Photogrammetry and Remote Sensing, 130, 13–31. https://doi.org/10.1016/j.isprsjprs.2017.05.010

Mahdianpari, M., Salehi, B., Rezaee, M. A., Mohammadimanesh, F., & Zhang, Y. (2018). *Very Deep Convolutional Neural Networks for Complex Land Cover Mapping Using Multispectral Remote Sensing Imagery.* Remote Sensing, 10(7), 1119. https://doi.org/10.3390/rs10071119

Mahdianpari, M. (2019). *Advanced machine learning algorithms for Canadian wetland mapping using polarimetric synthetic aperture radar (PolSAR) and optical imagery (Doctoral dissertation*, Memorial University of Newfoundland).

Mattia, F. (1997). *The effect of surface roughness on multifrequency polarimetric sar data.* IEEE Transactions on Geoscience and Remote Sensing, 35(4), 954–966. https://doi.org/10.1109/36.602537

Maxwell, AE, Warner, TA, & Fang, F (2018) *Implementation of machine-learning classification in remote sensing: an applied review,* International Journal of Remote Sensing, 39:9, 2784-2817,

DOI: 10.1080/01431161.2018.1433343

McFeeters, S. K. (1996). *The use of the Normalized Difference Water Index (NDWI) in the delineation of open water features.* International Journal of Remote Sensing, 17(7), 1425–1432. https://doi.org/10.1080/01431169608948714

Millard, K., & Richardson, M. (2015). *On the importance of training data sample selection in Random Forest image classification: A case study in peatland ecosystem mapping.* Remote Sensing, 7(7), 8489–8515. https://doi.org/10.3390/rs70708489

MoFE. (2018). *National Ramsar Strategy and Action Plan, Nepal (2018-2024).* Ministry of Forest and Environment. Singh Durbar, Kathmandu, Nepal.

Mohammadimanesh, F., Salehi, B., Mahdianpari, M., & Homayouni, S. (2016). *Unsupervised wishart classfication of wetlands in Newfoundland, Canada using polsar data based on fisher linear discriminant analysis.* International Archives of the Photogrammetry, Remote Sensing and Spatial Information Sciences - ISPRS Archives, 41, 305–310. https://doi.org/10.5194/isprsarchives-XLI-B7-305-2016

Pavlov, Y. L. (2019). *Random forests. Random Forests,* 1–122. https://doi.org/10.1201/9780429469275-8

Pekel, J. F., Cottam, A., Gorelick, N., & Belward, A. S. (2016). *High-resolution mapping of global surface water and its long-term changes.* Nature, 540 (7633), 418–422. https://doi.org/10.1038/nature20584

Ramsar Convention Secretariat. (2016). *The Fourth RAMSAR Strategic Plan 2016 - 2024.* Ramsar Handbooks for the Wise Use of Wetlands, 5th Edition, Vol. 2. Ramsar Convention Secretariat, Gland, Switzerland., v. 2(5. ed.), 1–54.

Rodriguez-Galiano, V. F., Ghimire, B., Rogan, J., Chica-Olmo, M., & Rigol-Sanchez, J. P. (2012). *An assessment of the effectiveness of a random forest classifier for land-cover classification.* ISPRS Journal of Photogrammetry and Remote Sensing, 67(1), 93–104. https://doi.org/10.1016/j.isprsjprs.2011.11.002

Roy, D. P., Ju, J., Kline, K., Scaramuzza, P. L., Kovalskyy, V., Hansen, M., Loveland, T. R., Vermote, E., & Zhang, C. (2010). *Web-enabled Landsat Data (WELD): Landsat ETM+ composited mosaics of the conterminous United States.* Remote Sensing of Environment, 114(1), 35–49. https://doi.org/10.1016/j.rse.2009.08.011

Sazib, N., Mladenova, I. E., & Bolten, J. D. (2018). *Leveraging the Google Earth Engine for Drought Assessment Using Global Soil Moisture Data.* Remote Sensing, 10(8), 1265. https://doi.org/10.3390/rs10081265

Shrestha, B., Shrestha, S., Shrestha, A., & Khadka, U. R. (2020). *Ramsar sites in Nepal: Conservation, present scenario, biodiversity value and threats.* Journal of Wetlands Ecology, 2020. 0-15. https://doi.org/10.3126/jowe.v2020i0.24782

Sun, S., Zhang, Y., Song, Z., Chen, B., Zhang, Y., Yuan, W., ... & Wang, Y. (2020). *Mapping coastal wetlands of the Bohai Rim at a spatial resolution of 10 M using multiple open-access satellite data and terrain indices.* Remote Sensing, 12(24), 4114. https://doi.org/10.3390/rs12244114

Survey, U. G. (2015). srtm Dem. *US Geological Survey.* https://earthexplorer.usgs.gov/

Tamiminia, H., Salehi, B., Mahdianpari, M., Quackenbush, L., Adeli, S., & Brisco, B. (2020). *Google Earth Engine for geo-big data applications: A meta-analysis and systematic review.* ISPRS Journal of Photogrammetry and Remote Sensing, 164, 152–170. https://doi.org/10.1016/j.isprsjprs.2020.04.001

Teluguntla, P., Thenkabail, P., Oliphant, A., Xiong, J., Gumma, M. K., Congalton, R. G., Yadav, K., & Huete, A. (2018). *A 30-m landsat-derived cropland extent product of Australia and China using random forest machine learning algorithm on Google Earth Engine cloud computing platform.* ISPRS Journal of Photogrammetry and Remote Sensing, 144, 325–340. https://doi.org/10.1016/j.isprsjprs.2018.07.017

Tian, H., Li, W., Wu, M., Huang, N., Li, G., Li, X., & Niu, Z. (2017). *Dynamic monitoring of the largest freshwater lake in China using a new water index derived from high spatiotemporal resolution sentinel-1A data.* Remote Sensing, 9(6), 6–9. https://doi.org/10.3390/rs9060521

Tyralis, H., & Papacharalampous, G. (2019). *Scientists and Practitioners and Their Recent History. Water.*

Van Beijma, S., Comber, A., & Lamb, A. (2014). *Random forest classification of salt marsh vegetation habitats using quad-polarimetric airborne SAR, elevation and optical RS data.* Remote Sensing of Environment, 149, 118–129. https://doi.org/10.1016/j.rse.2014.04.010

Wang, Y., Hess, L. L., Filoso, S., & Melack, J. M. (1995). *Understanding the radar backscattering from flooded and nonflooded Amazonian forests: Results from canopy backscatter modeling.* Remote Sensing of Environment, 54(3), 324–332. https://doi.org/10.1016/0034-4257(95)00140-9

Weiß, T. (2018). *SAR-pre-processing documentation.* https://buildmedia.readthedocs.org/media/pdf/multiply-sar-pre-processing/get_to_version_0.4/multiply-sar-pre-processing.pdf

Wilson, J. P., & Fothringgham, S. (2008). *The Handbook of Geographic Blackwell Companions to Geography.*

Xing, L., Tang, X., Wang, H., Fan, W., & Wang, G. (2018). *Monitoring monthly surface water dynamics of Dongting Lake using Sentinel-1 data at 10 m.* PeerJ, 2018(6), 1–22. https://doi.org/10.7717/peerj.4992

Xiong, J., Thenkabail, P. S., Gumma, M. K., Teluguntla, P., Poehnelt, J., Congalton, R. G., Yadav, K., & Thau, D. (2017). *Automated cropland mapping of continental Africa using Google Earth Engine cloud computing. ISPRS Journal of Photogrammetry and Remote Sensing,* 126, 225–244. https://doi.org/10.1016/j.isprsjprs.2017.01.019